Structural Engineering and Mechanics, Vol. 24, No. 6 (2006) 709-725
DOI: http://dx.doi.org/10.12989/sem.2006.24.6.709

Large deflection behavior and stability of slender bars under self weight

Paulo B. Gonçalves†

Civil Engineering Department, Catholic University, PUC-Rio, 22453-900 Rio de Janeiro, RJ, Brazil

Daniel Leonardo B. R. Jurjo‡, Carlos Magluta‡† and Ney Roitman‡†

Civil Engineering Department, Federal University of Rio de Janeiro, COPPE-UFRJ, 21941-972 Rio de Janeiro, RJ, Brazil

Djenane Pamplona‡†

Civil Engineering Department, Catholic University, PUC-Rio, 22453-900 Rio de Janeiro, RJ, Brazil

(Received May 8, 2006, Accepted July 25, 2006)

Abstract. In this paper the buckling and post-buckling behavior of slender bars under self-weight are studied. In order to study the post-buckling behavior of the bar, a geometrically exact formulation for the non-linear analysis of uni-directional structural elements is presented, considering arbitrary load distribution and boundary conditions. From this formulation one obtains a set of first-order coupled non-linear equations which, together with the boundary conditions at the bar ends, form a two-point boundary value problem. This problem is solved by the simultaneous use of the Runge-Kutta integration scheme and the Newton-Raphson method. By virtue of a continuation algorithm, accurate solutions can be obtained for a variety of stability problems exhibiting either limit point or bifurcational-type buckling. Using this formulation, a detailed parametric analysis is conducted in order to study the buckling and post-buckling behavior of slender bars under self-weight, including the influence of boundary conditions on the stability and large deflection behavior of the bar. In order to evaluate the quality and accuracy of the results, an experimental analysis was conducted considering a clamped-free thin-walled metal bar. As this kind of structure presents a high index of slenderness, its answers could be affected by the introduction of conventional sensors. In this paper, an experimental methodology was developed, allowing the measurement of static or dynamic displacements without making contact with the structure, using digital image processing techniques. The proposed experimental procedure can be used to a wide class of problems involving large deflections and deformations. The experimental buckling and post-buckling behavior compared favorably with the theoretical and numerical results.

Keywords: instability; post-buckling behavior; large deflections; self-weight; experimental analysis.

† Professor, Corresponding author, E-mail: paulo@civ.puc-rio.br
‡ Graduate Student
‡† Professor

1. Introduction

A survey of recent structures reveals a continuing trend towards longer and taller structures. Also structural elements are becoming lighter and thinner. Paradigmatic examples are flexible pipelines (risers) used in deep and ultra-deep offshore oil exploitation that may reach lengths of hundreds of meters. Their high slenderness ratio causes axial stiffness to be several orders of magnitude larger than the bending stiffness. This increases the importance of self-weight on the non-linear behavior and stability of these structures. In spite of its technical importance, the buckling and post-buckling behavior of columns under self-weight has not received the proper attention in the past. The linear stability analysis of clamped-free columns under self-weight was first analyzed by Greenhill (1881) who solved the linear equilibrium equation in terms of Bessel functions and determined the critical length. The derivation and solution of this problem can be found in Timoshenko and Gere (1961). Among the first large deflection analyses for this problem are the works of Frisch-Fay (1961), Schmidt and DaDeppo (1970), and Rao and Raju (1977), who studied the post-buckling of a uniform column subjected to a uniform axial-load using the Galerkin method. More recent studies of the problem include the works of Teng and Yao (2000), Maretic and Atanackovic (2001) Magnusson *et al.* (2001) and Lee (2001). These studies concentrated on the determination of critical loads and the post-buckling behavior of clamped-free columns. Tapered columns were analyzed by Li (2000) and Stuart (2001). The postbuckling and vibration of softening columns under self-weight was analyzed recently by Virgin and Plaut (2004). This problem had already been explored by Wang (1996).

The geometrically non-linear behavior and stability of uni-dimensional structural elements undergoing large deflections has been a topic of considerable interest in recent years due to its fundamental relevance to non-linear mechanics. This kind of problem finds applications in, for example, off-shore engineering, aerospace industry, suspension bridges, manufacture of robotic manipulators, construction of self erecting structures and manufacturing processes. For a few problems involving simple geometries and loading, mathematical solutions in terms of elliptic integrals are possible (Seide 1984). For more general problems, however, the use of numerical techniques is usually necessary.

This paper is concerned with a consistent one-dimensional treatment of the plane deformations of an initially straight or curved elastic thin-walled column under self weight that may experience large deflections and rotations along the post-buckling path (Antman 1995). Within the context of the assumptions of an extensible Bernoulli-Euler beam theory and using the standard methods of continuum mechanics, a geometrically exact set of first order non-linear equations in a Lagrangian framework is derived for a general curved-beam element. In order to obtain the equilibrium configurations, these equations are solved by the shooting method, which has been successfully used in the past for the numerical solution of non-linear boundary value problems (Keller 1968, Press *et al.* 1986). Here, the governing set of first-order differential equations is integrated numerically using the fourth-order Runge-Kutta method and the error in the boundary conditions is minimized by the Newton-Raphson algorithm. Equivalent formulations have been used in the past, but they are usually restricted to specific geometries and loading (Wolde-Tinsae and Foadian 1989, Lee *et al.* 1993).

In the analysis of slender one-dimensional structural elements, loss of stability and bifurcation are common phenomena and solution procedures that deal effectively with this class of problem are necessary. In structural mechanics, continuation methods have led to effective algorithms for

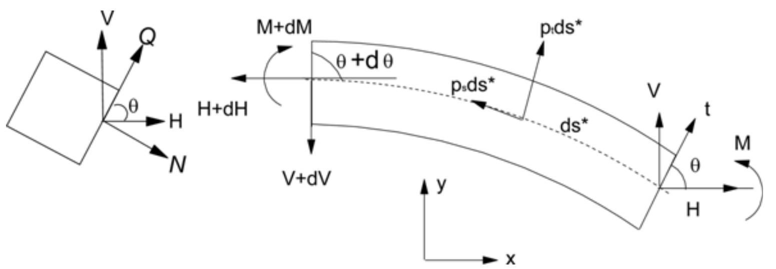

Fig. 1 Co-ordinate system and deformation of a typical point on centroidal axis

stability problems. In this paper, based on the seminal ideas of the continuation and homotopy methods (Lory 1980), some numerical procedures are derived and implemented to follow arbitrary non-linear equilibrium paths and identify turning and bifurcation points. The advantages of the present methodology are convenience for the designer and highly accurate numerical results. It could also be employed as a benchmark for other numerical methods and mechanical models.

Using these numerical tools, a detailed parametric analysis of the behavior of columns under self weight is conducted showing the variation of displacements and internal stress resultants along the pre- and post-buckling paths for different sets of boundary conditions.

In the experimental analysis of large deflections of very slender structures (involving small or large deformations) conventional measuring devices are usually not applicable, in particular those involving contact between the sensor and the structure. In some problems they may cause appreciable changes in mass and stiffness properties. They can also interact with the structure, leading to complex non-linear coupling. So, reliable non-contact techniques are preferable in such cases. A procedure appropriate for large deflection/large deformation problems is the use of image processing techniques (Pamplona *et al.* 2001, Jurjo *et al.* 2005, Pamplona *et al.* 2006). Here a detailed and precise experimental procedure is presented which can be effectively used in a large class of structural problems. Here this methodology is employed to analyze experimentally the buckling and post-buckling behavior of a thin-walled sheet of brass under self weight. The experimental results compare favorably with the results of the large-deflection analysis.

2. Large deflection analysis

Figs. 1 and 2 show the adopted co-ordinate systems as well as the undeformed configuration C_o and the deformed configuration C_n of an initially curved Euler-Bernoulli beam. In Figs. 1 and 2, the functions $x = x(s)$ and $y = y(s)$ of the curvilinear co-ordinate s represent the Cartesian components of the position of a typical point P along the undeformed centroidal axis, $u(s)$ and $w(s)$ are, respectively, the displacements in the x- and y-directions of point P due to deformation and t is the coordinate normal to the centroidal axis. In addition, θ_0 and θ are the slopes between the tangent to the beam curve and the y-axis and ds and ds^* are the length of an element in the undeformed and deformed configurations, respectively. Also, in Fig. 1 V and H are the vertical and horizontal forces, M is the bending moment and p_s and p_t are the load intensities per unit of deformed beam curve length in the tangential and normal directions respectively. A deformed element of a beam is shown in Fig. 2.

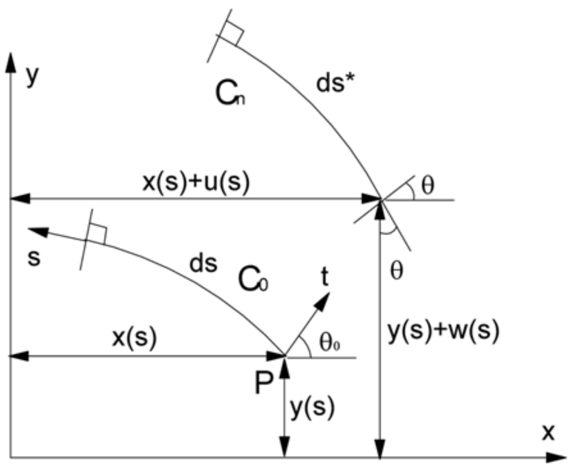

Fig. 2 Equilibrium of a beam element

From Fig. 1, the following basic set of geometric relations describing the undeformed configuration of a beam element can be written

$$dx/ds = -\sin\theta_0; \qquad dy/ds = \cos\theta_0 \tag{1}$$

As illustrated in Fig. 2, the deformed configuration can be described by the following kinematic relations

$$du/ds = -[(1+e)\sin\theta - \sin\theta_0]; \qquad dw/ds = [(1+e)\cos\theta - \cos\theta_0] \tag{2}$$

where $e = (ds^* - ds)/ds$ is the axial strain.

From the equilibrium of forces and moments, the following relations are derived.

$$\begin{aligned} dH/ds &= (1+e)[p_t\cos\theta - p_s\sin\theta] \\ dV/ds &= (1+e)[p_t\sin\theta + p_s\cos\theta] \\ dM/ds &= H(1+e)\cos\theta + V(1+e)\sin\theta \end{aligned} \tag{3}$$

The normal and shear forces on any cross section are given by (see Fig. 1)

$$N = H\sin\theta - V\cos\theta; \qquad Q = H\cos\theta + V\sin\theta \tag{4}$$

If the forces q_x and q_y per unit length of the undeformed centerline in the x and y directions are specified, then the forces p_s and p_t can be computed from

$$p_t = q_x\cos\theta + q_y\sin\theta; \qquad p_s = q_y\cos\theta - q_x\sin\theta \tag{5}$$

The derivatives of the loads, $dp_i/ds = \overline{p}(s)$, $i = t,s$, can be used as extra equations in the analysis.

The membrane stress resultant N and the bending stress resultant M are obtained in the usual way by integrating the stress over the cross section of the beam. Upon considering the quantities e, $d\theta_o/ds$, $d\theta/ds$ to be small relative to unity, one can write for a linearly elastic material that

$$N = \int_A \frac{R(s)_0}{R(s)_0 - t} EedA = EeA^*; \qquad M = \int_A t^2 \frac{R(s)_0}{R(s)_0 - t} E\kappa dA = E\kappa I^* \tag{6}$$

where E is the Young's modulus, A^* and I^* are the effective sectional properties of area and moment of inertia for the initially curved beam, $R(s)_0$ is the initial radius of curvature and κ is the bending curvature that is defined as

$$\kappa = -(d\theta/ds - d\theta_0/ds) \tag{7}$$

If $R(s)_0 >> t$, the approximations $A^* \cong A$, $I^* \cong I$ can be used to simplify the analysis.

From Eqs. (6) and (7), one obtains the differential equation

$$d\theta/ds = [(1/R(s)_0) - (M/EI^*)] \tag{8}$$

Eqs. (2), (3) and (8) form a set of six coupled non-linear ordinary differential equations having as independent variable the axial co-ordinate. These equations can be used to study non-linear in-plane deformation (including axial strain), buckling and post-buckling behavior of any straight or curved beam under in-plane loading conditions in the elastic range.

Solutions of the foregoing system must satisfy the following boundary conditions at the two boundaries ($s = s_1$; $s = s_2$)

$$\begin{aligned} H &= \overline{H} \quad \text{or} \quad u = \overline{u} \\ V &= \overline{V} \quad \text{or} \quad w = \overline{w} \\ M &= \overline{M} \quad \text{or} \quad \theta = \overline{\theta} \end{aligned} \tag{9}$$

where $(\overline{X}) = prescribed\ value.$

For curved beams of any shape it is usually more convenient to describe the undeformed centroidal arch as a function of the co-ordinate x. Using the differential relationship for the arc length $((ds)^2 = (dx)^2 + (df(x))^2)$, and the following relations

$$\begin{aligned} ds &= -dx[1 + (df(x)/dx)^2]^{1/2}; \qquad \theta(s)_0 = arctg\{[df(x)/dx]^{-1}\} \\ 1/R(s)_0 &= -[d^2f(x)/dx^2]/[1 + (df(x)/dx)^2]^{1/2} \end{aligned} \tag{10}$$

Eqs. (2), (3) and (8) can be easily written in terms of x.

2.1 Numerical method for the two-point boundary value problem

Only the basic ideas of the numerical methodology will be outlined, since the main procedures of the method can be found in the literature (Keller 1968, Press *et al.* 1986). The problem described by Eqs. (2), (3) and (8) and boundary conditions (9) is a non-linear two-point boundary value problem with three specified boundary conditions at each boundary. The shooting method reduces the solution of a boundary value problem (BVP) to the iterative solution of an initial value problem (IVP) (Keller 1968). This approach involves a trial-and-error procedure. At the starting point values are assumed for all variables and then the ODEs are solved by numerical integration, arriving at the other boundary. Unless the computed solution agrees with the known boundary conditions at this boundary, the initial conditions are adjusted and the process is repeated until the assumed initial conditions yield, within specified tolerances, a solution that agrees with the known boundary conditions.

So at $s = s_1$ only three variables among those shown in (9) are known. For the selection of the remaining three initial values, the shooting procedure will be used in combination with a root-finding technique. The procedure is as follows.

Eqs. (2), (3) and (8) can be written for integration purposes as

$$dY/ds = AY(s) + P \tag{11}$$

where $Y^T(s) = \{y_1, \ldots, y_6\} = \{u, w, \theta, H, V, M\}$.

Assume that three of the functions y_i are prescribed at $s = s_1$ and that three are prescribed at $s = s_2$. Therefore there are three freely specifiable starting values. Assume that these values are components of a vector S. The set of functions prescribed at s_1 will be denoted U_1 and those prescribed at s_2 by U_2. Given a particular trial vector $\overline{S}$ and U_1 the ODEs can be integrated from s_1 to s_2 as an IVP. Now, at $s = s_2$ a vector $F = \overline{U}_2 - U_2$, which measures the discrepancy between the prescribed values U_2 and the values obtained at the end point $\overline{U}_2$, is calculated. The components of F vanish if and only if all boundary conditions at s_2 are satisfied.

Now the Newton-Raphson method will be used to find the starting values s_i that zeros the discrepancies f_i at the other boundary. A correction vector ΔS can be found by solving the system of linear equations

$$J\Delta S = F \tag{12}$$

and an improved approximation is found by adding the correction back

$$\overline{S}_{i+1} = \overline{S}_i + \Delta S \tag{13}$$

It is not possible to compute the components $j_{ik} = \partial F_i / \partial s_k$ of the Jacobian matrix J analytically. Rather, each column of J requires a separate integration of the six ODEs, followed by the evaluation of the derivatives

$$\partial F_i / \partial s_k \cong [F_i(s_1, \ldots, s_k + \Delta s_k, \ldots) - F_i(s_1, \ldots, s_k, \ldots)] / \Delta s_k; \quad k = 1, 3 \tag{14}$$

Unless one starts quite far from the true values of S, it has been observed during the calculations that only two or three iterative cycles are usually required for convergence.

The procedure summarized above enables one to obtain a particular equilibrium configuration. In order to study the non-linear behavior and possible loss of stability of slender bars, the non-linear equilibrium paths should be obtained. For this continuation algorithms must be used in the analysis (Lory 1980). A continuation algorithm for stability analysis must include the capability of changing the control variables whenever necessary, here in addition to the load parameter, the non-homogeneous prescribed values and the free values at s_1 as well as the non-homogeneous prescribed values at s_2 which vary along the path with the load are used as control variables. To follow a given equilibrium path a control variable is chosen and when convergence fails due, for example, a limit point, a new variable is selected and this process is repeated until the desired path is obtained. The new variable is the one with the smoothest variation in the previous computations. This is an important difference of the present algorithm to those found in literature (Press *et al.* 1986).

3. Experimental methodology

In order to evaluate the quality and accuracy of the results, an experimental analysis was conducted considering a clamped-free thin-walled metal bar. As this kind of structure presents a high index of slenderness, its answers could be affected by the introduction of conventional sensors. In this paper, an experimental methodology was developed, allowing the measurement of static or dynamic displacements without making contact with the structure, using digital image processing techniques. This methodology uses only adhesive markers of negligible mass, facilitating the instrumentation for the experiment.

The experimental methodology here developed is divided into three stages:

(i) In the first stage, the image is captured by an analogical video camera.

(ii) In the second stage, the analogical image is converted to a digital image.

(iii) In the third stage, which is the most important one, the digital image is processed, with the objective of preparing it for the calibration and the reconstruction processes.

Using this methodology, it was possible to develop a computational vision system based on the programming language LabVIEW (version 6.1-National Instruments), which received the name Image-Sensor Program (ISP).

In the ISP, the processing routine consists of cutting the interest area of the image, decreasing the processing time and the noises outside the analysis area, limit it, turn gray level images into binary ones to enhance the interest points, and later, to identify the coordinates (u, v) of these points.

The computation of coordinates u and v of the points of interest in the image is made by transforming these points into small regions of interest, known in image processing as ROI (Regions of Interest). The ROI is characterized by a register (data set) that contains the contour coordinates of a determined region.

The interest points can be converted into ROIs by launching a “mask” onto the binary image. In the binary image only the interest points are in white color and the background is in black color. Thus, the mask identifies each one of the regions, looking for the border coordinates between black and white pixels. With the coordinates of the border it is possible to determine the central coordinates of each one of the regions. One of the main advantages of this process is that it can be performed with a great efficiency and low computational cost. Another advantage is associated with the small amount of information which has to be stored for each one of the images acquired along the time, which is an advantage, particularly in dynamics.

In order to allow the use of this system also in real time, the acquisition and processing routines in the ISP are executed in parallel. Thus, while the acquisition routine waits and digitizes an image, the processing routine segments (threshold), identifies and calculates the coordinates (u, v) of the interest points in the last digitized image.

The calibration is performed by identifying the coordinates u and v of the selected calibration points in the image by inserting their respective real coordinates (x and y), which are previously known. This process is done by the calibration routine in the ISP. After this selection, the values of the image coordinates are inserted automatically in a collection box by the ISP. The real coordinates are typed in this same box.

To obtain the transformation matrix, which correlates the real and the image coordinates, it is necessary to apply a suitable calibration method. There are several methods of calibration; the most used are: Direct Linear Transformation (DLT) (Abdel-Aziz and Karara 1971, Chen *et al*. 1994) and Tsai (1986). The method chosen for this study was the standard DLT, by virtue of the minimum level of distortions caused by the lenses of the video camera.

3.1 Calibration method

The DLT method is based on the underlying ideas of analytic photogrammetry, which has as its main objective to provide information about position, orientation and dimensions of objects in the space from the stereoscopic registers of its projections. The analytic photogrammetry is mainly based on the so called "Basic Equation of the Photogrammetry" or "Collinearity Equation" (Haralick and Shapiro 1993). This equation shows that, for any position of the camera in the space at the moment of the image capture, the luminous ray reflected by the point (x, y, z) describes a straight line passing through the position of the optical center of the camera. If the movements of a structure occur in a plane, as in the present case, the equation can be written only in terms of the x and y coordinates.

The "Collinearity Equation" that expresses the relation between the image coordinates (u, v) and its respective real ones (x, y) in the plane, are

$$\begin{aligned} xL_1 + yL_2 + L_3 - uxL_7 - uyL_8 &= u \\ xL_4 + yL_5 + L_6 - vxL_7 - vyL_8 &= v \end{aligned} \tag{15}$$

Coefficients L_1 to L_8 are the DLT calibration parameters, which correlate the real coordinates of a point in the plane (x, y) with its respective image coordinates (u, v). As shown in Eq. (15), each real point and its respective point in the image generates a pair of equations. In order to obtain the coefficients "L_i" it is necessary to expand this equation to n points:

$$\begin{bmatrix} x_1 & y_1 & 1 & 0 & 0 & 0 & -u_1x_1 & u_1y_1 \\ 0 & 0 & 0 & x_1 & y_1 & 1 & -v_1x_1 & -v_1y_1 \\ & & & & \vdots & & & \\ x_n & y_n & 1 & 0 & 0 & 0 & -u_nx_n & -u_ny_n \\ 0 & 0 & 0 & x_n & y_n & 1 & -v_nx_n & -v_ny_n \end{bmatrix} \begin{bmatrix} L_1 \\ L_2 \\ \vdots \\ L_7 \\ L_8 \end{bmatrix} = \begin{bmatrix} u_1 \\ v_1 \\ \vdots \\ u_n \\ v_n \end{bmatrix} \tag{16}$$

As the number of unknowns is equal to 8 (DLT parameters), at least 4 calibration points (8 equations) are necessary to obtain coefficients "L_i". To minimize the error it is possible to use more than 4 calibration points. In this case the system of linear equations obtained cannot be directly resolved, since it is over-determined.

This problem can, however, be solved using the least-squares method, minimizing the errors. The application of the least-squares method to Eq. (16) leads to

$$A_{2n\,x\,8}\,.\;L_{8\,x\,1} = B_{2n\,x\,1} \tag{17}$$

Multiplying both sides of Eq. (17) by the transposed of matrix A will result in:

$$C_{8x8}\,.\;L_{8x1} = D_{8x1} \tag{18}$$

The calibration coefficients are obtained by solving Eq. (18). However, Eq. (15) cannot directly be used for the reconstruction. Manipulating again Eq. (15), the coordinates (x, y) are obtained from the following equation:

$$\begin{bmatrix} L_1^{(1)} - u^{(1)}L_7^{(1)} & L_2^{(1)} - u^{(1)}L_8^{(1)} \\ L_4^{(1)} - v^{(1)}L_7^{(1)} & L_5^{(1)} - v^{(1)}L_8^{(1)} \end{bmatrix} \begin{bmatrix} x \\ y \end{bmatrix} = \begin{bmatrix} u^{(1)} - L_3^{(1)} \\ v^{(1)} - L_6^{(1)} \end{bmatrix} \tag{19}$$

This system has a unique solution using just one camera. However, the errors in the coordinate values can be minimized if several cameras are used. In this case, the coordinates (x, y) are obtained from:

$$\begin{bmatrix} L_1^{(1)} - u^{(1)}L_7^{(1)} & L_2^{(1)} - u^{(1)}L_8^{(1)} \\ L_4^{(1)} - v^{(1)}L_7^{(1)} & L_5^{(1)} - v^{(1)}L_8^{(1)} \\ \vdots & \vdots \\ L_1^{(m)} - u^{(m)}L_7^{(m)} & L_2^{(m)} - u^{(m)}L_8^{(m)} \\ L_4^{(m)} - v^{(m)}L_7^{(m)} & L_5^{(m)} - v^{(m)}L_8^{(m)} \end{bmatrix} \begin{bmatrix} x \\ y \end{bmatrix} = \begin{bmatrix} u^{(1)} - L_3^{(1)} \\ v^{(1)} - L_6^{(1)} \\ \vdots \\ u^{(m)} - L_3^{(m)} \\ v^{(m)} - L_6^{(m)} \end{bmatrix} \tag{20}$$

The solution of Eq. (20) can also be obtained by applying the least-squares method. For this, Eq. (20) can be re-written as:

$$E_{2mx2}\,.\;R_{3x1} = F_{2mx1} \tag{21}$$

where m is the number of cameras.

Eq. (21) results in an over-determined system, which can be solved by applying again the least-square method, i.e., by multiplying Eq. (21) by the transpose of matrix E, resulting in:

$$G_{2x2}\,.\;R_{2x1} = H_{2x1} \tag{22}$$

3.2 Experimental apparatus

For the dynamic experimental analysis of a clamped-free slender column under self-weight, a special device was developed, as shown in Fig. 3. This apparatus is composed of the following items:

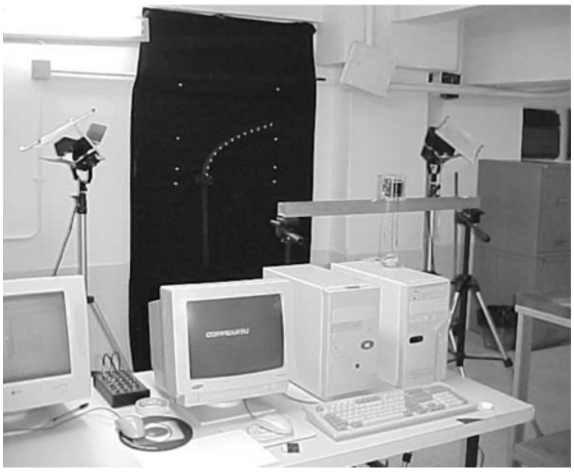

Fig. 3 Experimental apparatus used in the analysis

(a) Two analogical video camera with NTSC system and CCD of ¼ inch, with a total of 811(H) × 508 (V) CCD pixels. These cameras present a scanning system of 525 lines with 60 frames/second, resolution of 470 TV Lines, electronic shutter with 1/120000 seconds, manual and automatic focus, Cannon lenses with 22X of optical zoom and 220X of digital zoom and focal distance varying from 3.7 to 85.1 mm;
(b) A personal computer with the ISP and the monochromatic frame grabber (PCI-1409/National Instruments);
(c) A special illumination system composed of light bulbs without oscillation, with the purpose of keeping a uniform illumination on the object to be analyzed;
(d) A metallic sheet of brass representing a slender column with width b = 9.0 cm; thickness h = 0.45 mm; load per unit length (self-weight) q = 3.43 N/m; Young's Modulus E = 123257 MPa (mean values of the experimental results); and variable length (30 – 70 cm).

For this experimental analysis, a black color background, illustrated in Fig. 3, was used in order to minimize the noises. Other advantage of this strategy is to facilitate the image processing and, mainly, to eliminate the shades projected on the background by the column.

In this analysis, to represent the interest points, small white color rectangular adhesives of negligible mass were used as markers. These adhesives were placed along the length of the columns and on the background, in order to perform the calibration process. As can be seen in Fig. 3, eight calibration points were used.

Table 1 Buckling loads for selected sets of boundary conditions

Clamped-free column	$(qL)_{cr} = 7.83\ EI/L^2$
Simply supported	$(qL)_{cr} = 18.57\ EI/L^2$
Clamped-simply supported	$(qL)_{cr} = 33.03\ EI/L^2$
Clamped-clamped	$(qL)_{cr} = 49.44\ EI/L^2$

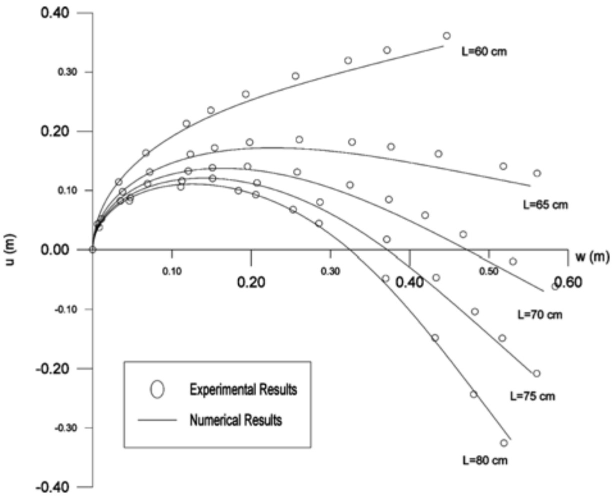

Fig. 4 Clamped-free column. Comparison between numerical and experimental results

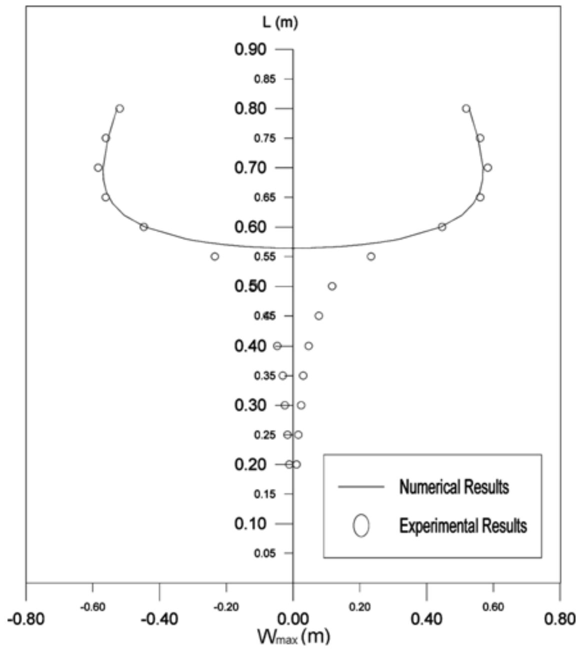

Fig. 5 Post-buckling path of a clamped-free column. Comparison between numerical and experimental results

4. Results and discussion

Timoshenko and Gere (1961) solved the problem of a clamped-free column under self-weight in terms of Bessel functions. The critical load is shown in the first line of Table 1. Jurjo (2001) obtained the critical load of a heavy column under different sets of boundary conditions using the Rayleigh-Ritz method and symbolic algebra. The results are shown in Table 1. Considering that the axial load per unit length q is constant, the problem is to find the critical length, L_{cr}, of the column and the influence of an increasing length on the post-buckling behavior of the column.

The theoretical critical length for the clamped-free column used in the experiments is l_{cr} = 56.44 cm, which agrees with the experimental result. The comparison of the experimentally obtained deformed shapes with the numerical results is shown in Fig. 4, for selected bar lengths. The maximum deflection as a function of the beam length is plotted in Fig. 5, where the experimental results are compared with the post-buckling path obtained numerically. As observed, there is a reasonable agreement between the experimental and numerical results. The small difference near the critical

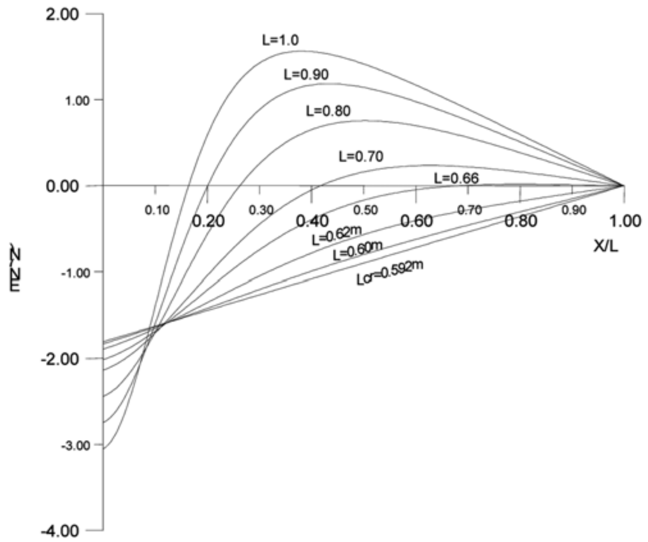

Fig. 6 Clamped-free column. Variation of normal forces for increasing bar lengths

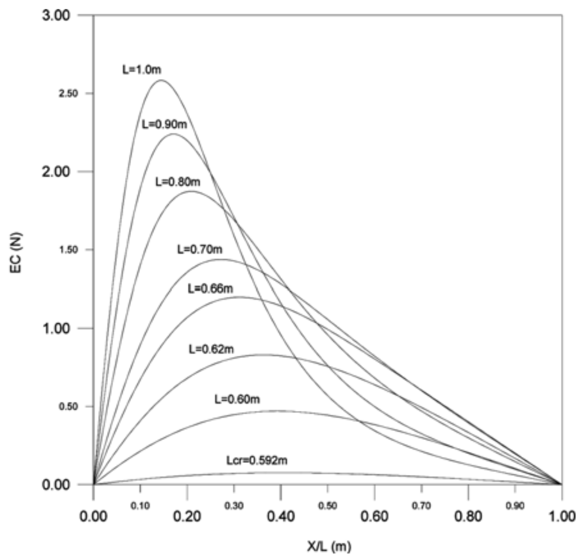

Fig. 7 Clamped-free column. Variation of shear forces for increasing bar length

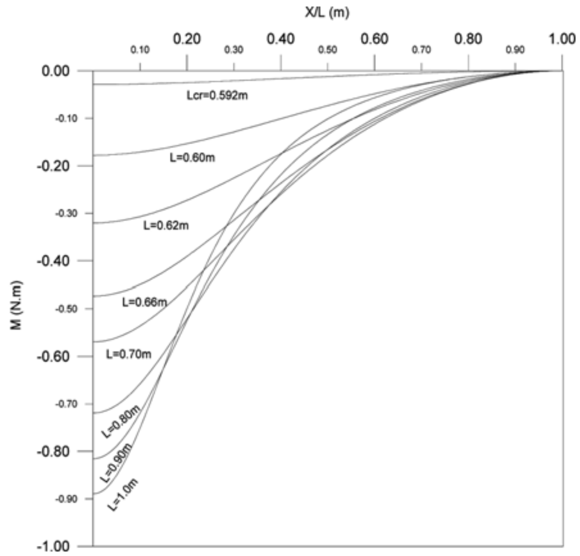

Fig. 8 Clamped-free column. Variation of bending moments for increasing bar length

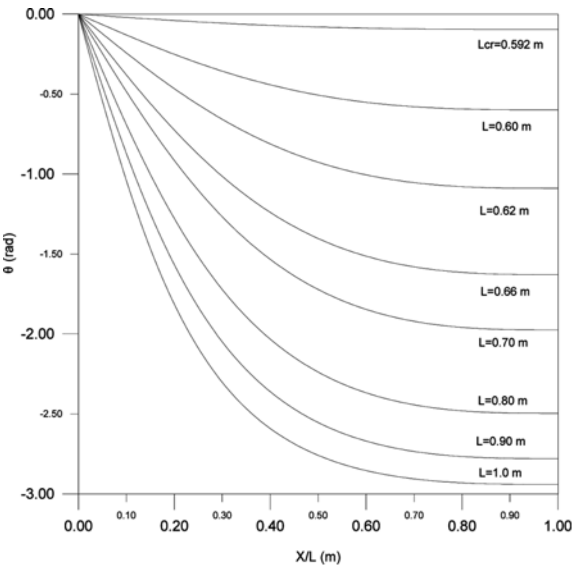

Fig. 9 Clamped-free column. Variation of the rotation for increasing bar length

load is typical of columns and is due to small geometric imperfections.

Figs. 6 to 8 illustrate the variation of the stress resultants (normal and shear forces and bending moment) along the bar axis for increasing column length. They are rarely shown in the literature in spite of being the most important variables in design. As observed in Fig. 6, for $l \leq l_{cr}$, the normal force varies linearly. After buckling, as the length increases, the beam deforms and the compressive force decreases along the upper part of the beam and increases slightly near the support. After a certain critical length (here $l = 0.65$ cm) an increasing portion of the column is under tension while

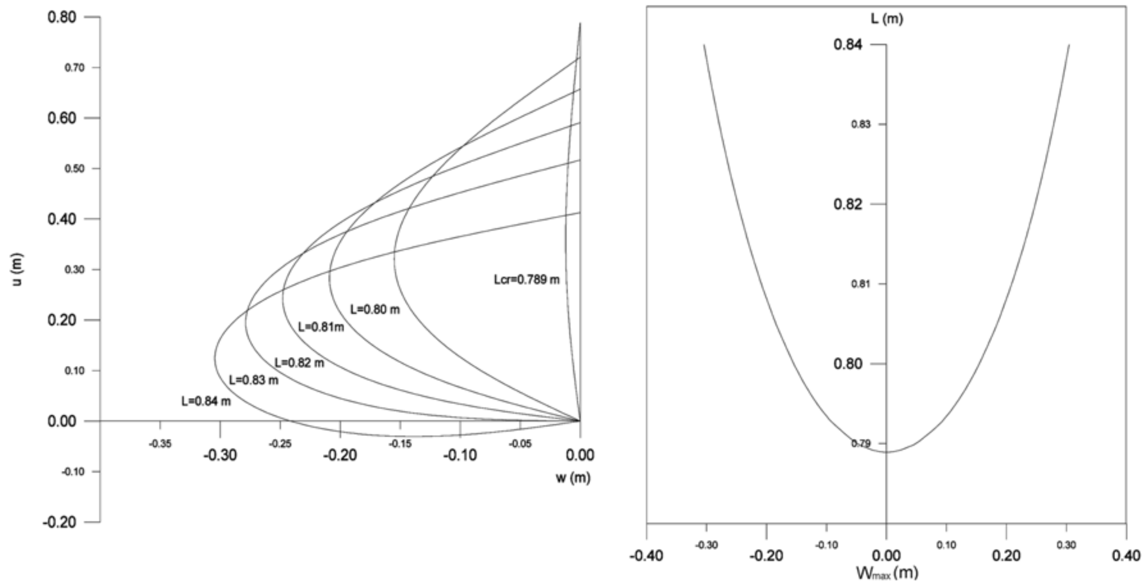

Fig. 10 Simply supported column. Deformed column and post-buckling path

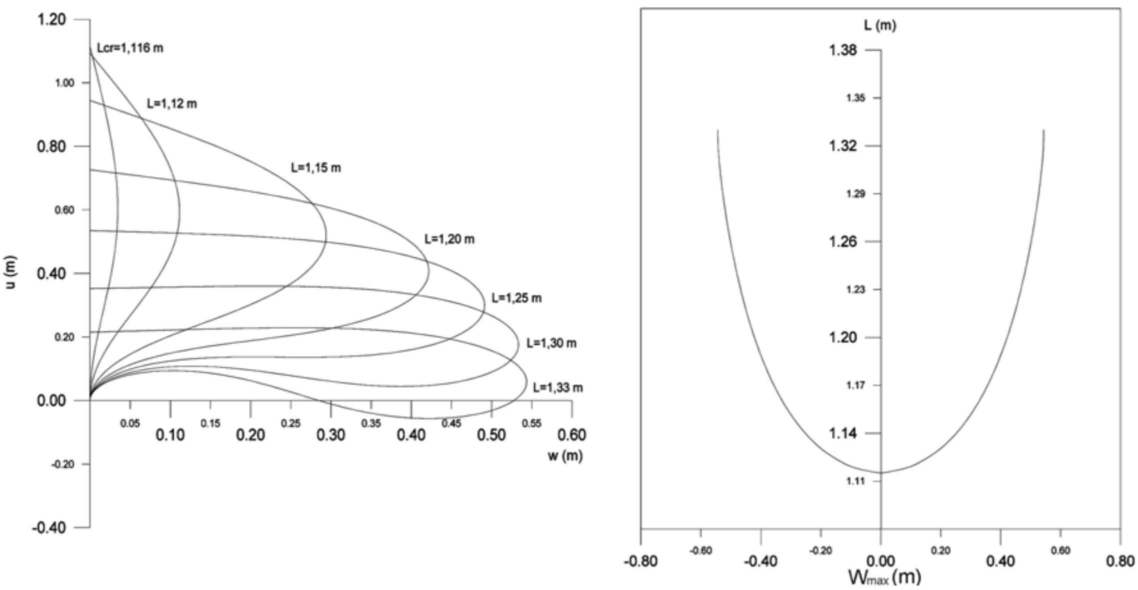

Fig. 11 Clamped-simply supported column. Deformed column and post-buckling path

the compression still increases, as expected, since the length is increasing, near the support. As the column deforms, shear forces and bending moments, which are zero before buckling, increase steadily in a non-linear manner, as shown in Figs. 7 and 8. While shear is always zero at both ends, reaching a maximum value along the lower half of the bar, the bending moment increases exponentially reaching the maximum value at the support. In general the internal forces are so

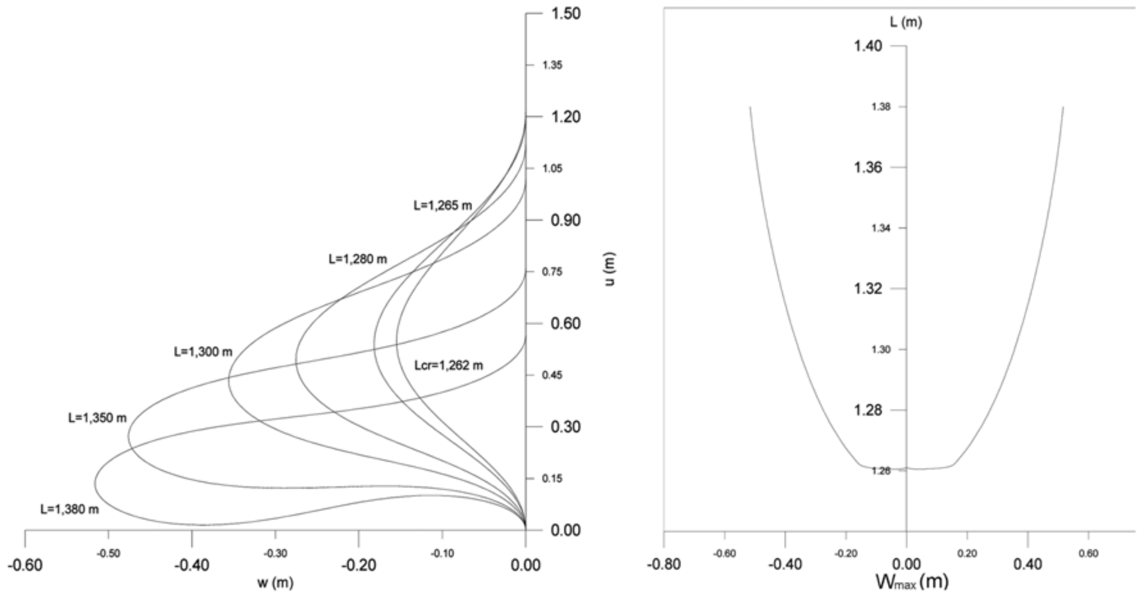

Fig. 12 Clamped-clamped column. Deformed column and post-buckling path

nonlinear that any linear approximation is meaningless. The complex variation of stress resultants along the beam emphasizes the importance of a detailed non-linear large deflection analysis of long slender bars under self-weight. The variation of the rotation θ is shown in Fig. 9. All these results are obtained directly from the integration procedure. This is one of the advantages of the present formulation over more traditional displacement formulations were stresses are derived from an approximate displacement field and have consequently a lower degree of accuracy.

Figs. 10 to 12 show (a) the deformed shapes and (b) the post-buckling path of a column for three different sets of boundary conditions. In all cases analyzed in this paper, the column exhibits a supercritical bifurcation and a symmetric stable post-buckling path with a high degree of effective stiffness, much higher than the classical Euler column under end point load. Although the boundary conditions have a noticeable influence on the critical load and on the stress distribution, their influence on the shape of the post-buckling solution is small. It is interesting to notice that for columns buckling under self-weight, even for lengths slightly higher than the critical one, large deflections are already present.

4. Conclusions

In this paper the non-linear behavior and instability of columns under self weight was analyzed in detail. Particular attention was given to the large deflection post-buckling behavior of the bar. In order to study this problem, general non-linear differential equations governing the behavior of thin prismatic bars of arbitrary initial shape and subjected to arbitrary loading and boundary conditions have been derived. A numerical methodology based on the underlying ideas of the shooting and continuation method is proposed, in which the boundary conditions and control variables can be changed whenever desired. This enables one to obtain complex equilibrium paths exhibiting bifurcation and limit points and, consequently, study the equilibrium and stability characteristics of a variety of important engineering problems. To verify the numerical results, an experimental analysis of a thin clamped-free bar under self-weight was conducted. A detailed and precise experimental procedure appropriate for large deflection/large deformation problems based on image processing techniques is presented which can be effectively used in a large class of structural problems, in particular, problems where conventional experimental techniques may have an effect on the results. It is shown that the numerical and experimental results are in good agreement. The results also show the influence of self-weight and large deflections on the load carrying capacity and internal force distribution of columns with different sets of boundary conditions.

References

Abdel-Aziz, Y.I. and Karara, H.M. (1971), "Direct linear transformation from comparator coordinates into object space coordinates in close-range photogrammetry", *Proc. of the Symposium on Close-Range Photogrammetry*, Falls Church, VA: American Society of Photogrammetry, 1-18.

Antman, S.S. (1995), *Nonlinear Problems of Elasticity*, Springer-Verlag, New York, USA.

Chen, L., Armstrong, C.W. and Raftopoulos, D.D. (1994), "An investigation on the accuracy of three-dimensional space reconstruction using the direct linear transformation technique", *J. Biomechanics*, **27**, 493-500.

Frisch-Fay, R. (1961), "The analysis of a vertical and a horizontal cantilever under a uniformly distributed load", *J. Franklin Inst.*, **271**, 192-199.

Greenhill, A.G. (1881), "Determination of the greatest height consistent with stability that a vertical pole or mast can be made, and of the greatest height to which a tree of given proportions can grow", *Proc. Camb. Phil. Soc.*, **4**, 65-73.

Haralick, R.M. and Shapiro, L.G. (1993), *Computer and Robot Vision*, Vol. 2. Addison-Wesley Publishing Company.

Jurjo, D.L.B., Magluta, C., Roitman, N. and Gonçalves, P.B. (2005), "Dynamic analysis of columns under self-weight", *26th Iberian Latin American Congress on Computational Methods in Engineering*, XXVI CILAMCE, Brazil, 1-10.

Jurjo, D.L.B. (2001), "Buckling and post-buckling of a heavy column under self-weight", MSc Dissertation, Catholic University, PUC-Rio, Rio de Janeiro, Brazil.

Keller, H.B. (1968), *Numerical Methods for Two-point Boundary Value Problems*, Blaisdell Publishing Company, Waltham, Mass., USA.

Lee, B.K., Wilson, J.F. and Bolle, N.A. (1993), "Elastica of cantilevered beams with variable cross sections", *Int. J. Non-Linear Mech.,* **28**, 579-589.

Lee, K. (2001), "Post-buckling of uniform cantilever column under combined load", *Int. J. Non-Linear Mech.*, **36**, 813-816.

Li, Q.S. (2000), "Exact solutions for buckling of non-uniform columns under axial concentrated and distributed loading", *Eur. J. Mech.* A, **20**, 485-500.

Lory, P. (1980), "Enlarging the domain of convergence for multiple shooting by the homotopy method", *Numer. Math.*, **35**, 231-240.

Maretic, R.B. and Atanackovic, T.M. (2001), "Buckling of column with base attached to elastic half-space", *J. Eng. Mech.*, ASCE, **127**(3), 242-247.

Margusson, A., Ristinmaa, M. and Ljung, C. (2001), "Behavior of the extensible elastica solution", *Int. J. Solids Struct.,* **38**, 8441-8457.

Pamplona, D., Gonçalves, P.B., Davidovitch, M. and Weber, H.I. (2001), "Finite axisymmetric deformations of a initially stressed fluid-filled cylindrical membrane", *Int. J. Solids Struct.,* **38**, 2033-2047.

Pamplona, D.C., Gonçalves, P.B. and Lopes, S.R.X. (2006), "Finite deformations of cylindrical membrane under internal pressure", *Int. J. Mech. Sci.*, **48**, 683-696.

Press, W.H., Flannery, B.P., Teukolsky, S.A. and Vetterling, W.T. (1986), *Numerical Recipes*. Cambridge University Press, UK.

Rao, G.V. and Raju, P.C. (1977), "Post-buckling of uniform cantilever column – Galerkin finite element solution", *Eng. Fract. Mech.*, **1**, 1-4.

Schmidt, R. and DaDeppo, D.A. (1970), "Large deflection of heavy cantilever beams and columns", *Quart. Appl. Math.*, **28**, 441-444.

Seide, P. (1984), "Large deflection of a simply supported beam subjected to moment at one end", *J. Appl. Mech.*, ASME, **51**, 519-525.

Stuart, C.A. (2001), "Buckling of a heavy tapered rod", *J. Math. Pures Appl.*, **80**, 281-337.

Teng, J.G. and Yao, J. (2000), "Self-weight buckling of FRP tubes filled with wet concrete", *Thin-Walled Structures*, **38**, 337-353.

Timoshenko, S.P. and Gere, J.M. (1961), *Theory of Elastic Stability*, Mc Graw-Hill, New York, USA.

Tsai, R.Y. (1986), "An efficient and accurate camera calibration technique for 3D machine vision", *Proc. of IEEE Conf. on Computer Vision and Pattern Recognition*, Miami Beach, Florida, USA, 364-374.

Virgin, L.N. and Plaut, R.H. (2004), "Postbuckling and vibration of linearly elastic and softening columns under self-weight", *Int. J. Solids Struct.*, **41**, 4989-5001.

Wang, C.Y. (1996), "Global buckling load of a nonlinearly elastic bar", *Acta Mech.*, **119**, 229-234.

Wolde-Tinsae, A.M. and Foadian, H. (1989), "Asymmetrical buckling of prestressed tapered arches", *J. Eng. Mech.*, ASCE, **115**, 2020-2034.